



DOI: 10.24874/ti.2093.12.25.03

Tribology in Industry

www.tribology.rs



Comparative Analysis of Cutting Forces, Surface Roughness, and Chip Morphology in Conventional and Hard Turning of 100Cr6 Steel Using CC650 Ceramic Inserts

Faouzi Hamza^{a,*}, Abdelmoumene Guedri^b, Hamid Hamadache^c

^aDepartment of Geotechnology, Mining Institute, Larbi Tebessi University, 12000, Tebessa, Algeria.

^bDepartment of Mechanical Engineering, INFRA-RES Laboratory, Mohammed Chérif Messaadia University, Souk Ahras, Algeria.

^cDepartment of Mechanical Engineering, LRATPM Laboratory, Badji Mokhtar-Annaba University, Annaba, Algeria.

Keywords:

Cutting parameters
Cutting forces
Surface roughness
Chip morphology
100Cr6 steel
CC650 ceramic inserts

* Corresponding author:

Faouzi Hamza
E-mail: faouzi-hamza@hotmail.fr

Received: 13 December 2025

Revised: 3 February 2026

Accepted: 6 March 2026



ABSTRACT

Cutting parameters, the mechanical behavior of the workpiece material, and cutting tool wear strongly affect cutting forces and surface roughness, and consequently the quality of the machined product. This work investigates metal cutting under both conventional and hard turning conditions by analyzing the evolution of cutting forces and surface roughness during the machining of 100Cr6 bearing steel, before and after hardening to 60 HRC, using a CC650 ceramic insert. The study examines the influence of cutting speed, feed rate, and depth of cut on the cutting force components (F_a , F_r , and F_v) and surface roughness parameters (R_a , R_t , and R_z) using a unifactorial experimental approach. By analyzing the curves that summarize the numerical trends, the evolution of cutting forces and surface roughness was compared for identical cutting parameter levels in both conventional and hard turning. Additionally, chip morphology was investigated to provide further insight into the plastic deformation of the material. Response modeling was performed to relate the cutting force components and surface roughness parameters to the input variables (V_c , f , and a_p). Results show that conventional turning generates significantly higher cutting forces than hard turning, with maximum increases of 100% (F_a), 75% (F_r), and 90% (F_v), differences that reduce with increasing depth of cut. Conversely, hard turning yields superior surface integrity, achieving peak improvements of 464% (R_a), 137% (R_t), and 161% (R_z) over conventional methods at a cutting speed of 260 m/min.. Chip morphology analysis further illustrates the influence of cutting parameters on the plastic deformation behavior of the material in both machining processes.

© 2026 Published by Faculty of Engineering

1. INTRODUCTION

Hard turning is a machining process that consists of shaping hardened components using high-performance cutting tools capable of removing material from hard steels, alloys, or certain composite materials. This process presents specific challenges due to the high hardness of the workpiece and the resulting demand on the wear resistance of the cutting tool. In such applications, cutting tools made from cemented carbides, ceramics, or cubic boron nitride (CBN) are typically required, as these materials can withstand the elevated temperatures and wear generated during machining. In addition, cutting parameters such as cutting speed, feed rate, and depth of cut must be carefully selected to maintain tool integrity and ensure process stability. Hard turning is widely used in sectors such as aerospace, automotive, and precision component manufacturing, where tight dimensional tolerances and high-quality surface finishes are essential. According to the definition provided by Kumar et al. [1], hard turning consists of machining hardened parts (45–65 HRC) using defined-geometry cutting tools, thus advantageously replacing grinding operations.

Several studies on steel machining have highlighted the advantages and specificities of hard turning. Lalwani et al. [2] experimentally investigated the influence of cutting parameters on cutting forces and surface roughness during the hard turning of MDN250 steel using a coated ceramic tool. Sahbi et al. [3] optimized the hard turning of AISI 4140 steel with a ceramic insert using a Taguchi L9 design, applying multi-objective optimization to minimize surface roughness and tool wear while maximizing the material removal rate. Lakić et al. [4] examined high-pressure jet-assisted machining in the hard turning of 100Cr6 bearing steel (62 HRC) with coated carbide tools, demonstrating improved productivity, extended tool life, reduced wear, and acceptable surface roughness. Umamaheswarrao et al. [5] analyzed the effects of cutting parameters, tool geometry (nose radius and cutting angle), and surface defects on machining forces in both hard and conventional turning of AISI 52100 steel. Ibraheem [6] developed an artificial neural network model to predict machining forces as a function of cutting parameters and workpiece hardness during the

machining of AISI 52100 steel. Aouici et al. [7] studied the effects of cutting speed, feed rate, depth of cut, and workpiece hardness on surface roughness and cutting force components in hard turning. Bartarya et al. [8] examined the influence of cutting parameters on cutting forces and surface roughness during hard turning of AISI 52100 steel. Boy et al. [9] experimentally investigated and modeled surface roughness and cutting forces in the hard turning of AISI H13 steel. Azizi et al. [10] modeled cutting forces and surface roughness to optimize machining conditions in the hard finishing of AISI 52100 steel. Tuan et al. [11] evaluated the influence of MoS₂ nanofluid MQL parameters on cutting forces and surface roughness during hard turning with a CBN insert. Çetindağ et al. [12] investigated hybrid and cryogenic lubrication methods and their effects on surface integrity (surface roughness, microhardness, and residual stresses) during the hard turning of AISI 52100 steel (62 HRC) with CBN inserts. Hamadi et al. [13] assessed tool performance, including insert wear, surface roughness, cutting forces, cutting power, and material removal rate, during the dry turning of AISI 4140 with three coated carbide grades. Thangarasu et al. [14] predicted tool wear in hard turning of EN8 steel using cutting force and surface roughness through an artificial neural network. Osička et al. [15] analyzed cutting forces and surface roughness as a function of cutting parameters when machining hardened 100Cr6 steel with a CBN tool. Özdemir et al. [16] studied the effects of cutting parameters on surface roughness and cutting forces during the hard turning of 42CrMo4 steel using a ceramic insert. Kumar et al. [17] investigated the performance of mixed ceramic inserts under accelerated cooling, demonstrating significant improvements in tool life and surface integrity during hard turning. The research further optimizes cutting parameters to enhance efficiency and sustainability in high-performance machining environments. Mane et al. [18] modeled and optimized the radial cutting force (F_r) using the response surface method during dry hard turning of AISI 52100 steel. Das et al. [19] evaluated the influence of cutting parameters on cutting forces and surface roughness during dry hard turning of AISI 52100 using a CBN tool. Balwan et al. [20] investigated the effects of speed, depth of cut, tool nose radius, hardness,

and feed rate on cutting forces when turning EN353 hardened steel with a CBN insert. Kumar et al. [21] examined hard turning of AISI D2 steel (46 HRC) using CBN inserts, considering cutting force and surface roughness as response variables. Ngol [22] studied the influence of nanoparticle concentration, pressure, and air flow rate on total cutting force in hard turning using NF-MQL and NF-MQCL lubrication with nanofluids, identifying optimal conditions for minimizing cutting forces. Finally, Kumar et al. [23] investigated tool wear and surface characteristics during hard turning of AISI D2 steel (55 ± 1 HRC) with coated carbide tools under air-water jet spray impingement cooling, reporting acceptable surface roughness, reduced cutting temperature (maximum 200.6 °C), and a tool life of 20.3 minutes under optimal conditions. To overcome the limitations of traditional machining, several advanced strategies have been explored in recent years. For instance, Wang et al. [24] developed a bio-inspired approach using Nepenthes-shaped micro-textures to optimize lubricant transport, effectively reducing friction at the tool-chip interface. In parallel, Sun et al. [25] investigated the heat transfer mechanisms in coated tools using the finite difference method to predict temperature fields in sustainable turning. Additionally, Shi et al. [26] analyzed the use of solid additives to strengthen ceramic cutting tools, providing a methodology to enhance tool life when machining hardened materials. These innovations emphasize the critical role of thermo-mechanical control, a factor that remains central to this comparative study between annealed and hardened 100Cr6 steel. In the quest for sustainable and high-performance manufacturing, recent studies have explored innovative lubrication and tool design strategies. For instance, Wang et al. [27] investigated the tribological performance of enhanced turning using biolubricants, providing a comparative assessment that highlights the potential for eco-friendly cooling solutions. Furthermore, to address tool wear, Gong et al. [28] analyzed the lubricant transportation mechanism and wear resistance of textured tools with different micro-arrangement patterns. These studies emphasize that controlling the tool-workpiece interface through either advanced lubrication or surface engineering is vital for extending tool life and improving surface integrity.

The scientific literature provides a broad foundation for understanding these processes. Significant contributions have been made by several researchers [29–35] who focused on the experimental and analytical modeling of cutting forces, highlighting the influence of tool geometry and material hardness. Similarly, the evolution of surface finish and topographic integrity in hard turning has been extensively addressed in recent studies [36–42], emphasizing the transition from conventional to precision machining. Furthermore, the complex mechanisms governing chip morphology, such as adiabatic shear banding and segmentation, have been thoroughly explored by [43–48], providing a physical basis for the observed thermo-mechanical phenomena in high-strength alloys.

Extensive literature exists on the benefits of hard turning over grinding. However, a significant research gap remains regarding the direct experimental comparison between conventional and hard turning under identical cutting conditions. Most existing studies focus on the transition from grinding to hard turning, leaving a lack of systematic data on how the same tool material and parameters behave across different hardness levels. To address this gap, the main objective of this study is to experimentally evaluate and quantify the influence of cutting parameters (V_c, f, ap) on cutting force components (F_i) and surface roughness (R_i) during the machining of 100Cr6 steel in both its annealed and quenched (60 HRC) states using CC650 ceramic inserts. The innovation of this work resides in the identification of the thermo-mechanical inversion points and the development of mathematical models to predict these outputs, providing a robust tool for process optimization. A distinctive feature of this work is the correlation between chip morphology through photographic analysis and the underlying deformation mechanisms that distinguish conventional from hard turning. This comprehensive approach provides a systematic assessment of hard turning's performance, confirming its role as an efficient substitute for traditional finishing processes on an industrial scale.

2. EXPERIMENTAL METHOD

This section details the experimental framework designed to compare the machining behavior of 100Cr6 steel in its annealed and hardened states. It describes the metallurgical properties of the workpiece, the characteristics of the ceramic tooling, and the systematic experimental design used to capture the influence of cutting parameters on process outputs. The following subsections provide the technical specifications for each component of the experimental setup.

The experiments were performed on cylindrical specimens of 100Cr6 steel (also known as AISI 52100), a material widely used in the manufacture of balls, rollers, rings, and bearing cages. It is also employed in cold-forming applications such as forming dies, rolling mill rolls, and wear-resistant liners. The chemical composition and mechanical properties of the material are presented in Table 1. Before heat treatment, the steel exhibited a hardness of 29 HRC. After quenching at 850 °C followed by tempering at 220 °C, the required hardness of 60 HRC was achieved.

The tensile and fatigue properties of this steel grade are difficult to evaluate because of its high brittleness and sensitivity to notching. For this reason, it is commonly characterized through compression and contact fatigue tests. In rolling contact fatigue, its endurance limit can be up to ten times higher than that of aluminum alloys.

Table 1. Chemical composition and mechanical properties of 10Cr6 steel.

Material	Chemical composition [%]			
	C	Si	Mn	P
0.93-1.05	0.15-0.35	0.25-0.45	≤0.025	
S	Cr	Ni	Mo	
≤0.03	1.35-1.60	0.21	≤0.1	
100Cr6 EN 10027	Mechanical properties			
	E (Gpa)	Re (Mpa)	Rm (Mpa)	Rp0.2 (Mpa)
	210	550-850	750-850	≥500
	A%	ν	Hadness	Density
	10-13	0.3	29-33	7.83

The test specimen used in this study is a cylindrical bar with a diameter of 60 mm and a length of 350 mm, from which several 20 mm-wide bearing sections separated by 5 mm grooves were machined. This configuration enables multiple tests to be conducted on the same bar. Figure 1 presents the geometry and a photograph of the test specimen.

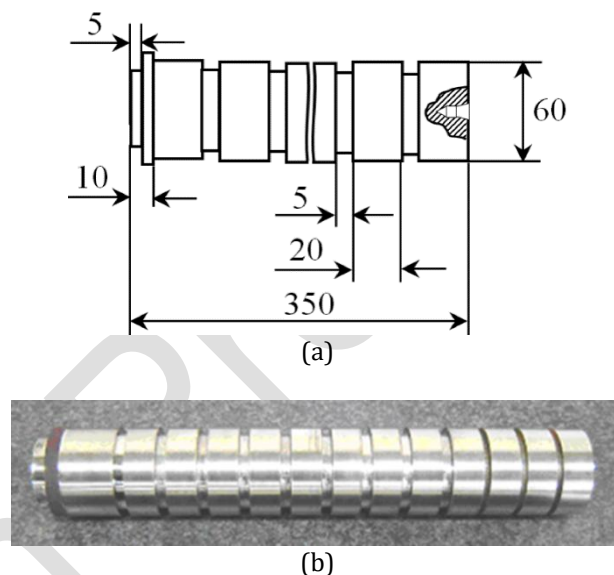


Fig. 1. Specimen, (a) geometry and (b) photograph.

The cutting inserts used in this study are removable, square-shaped inserts mounted on the insert holder using a combined wedge and pin clamping system (Fig. 2a and Fig. 2b). A screwed and ground carbide support wedge protects the tool holder while ensuring optimal contact between the insert and the holder.

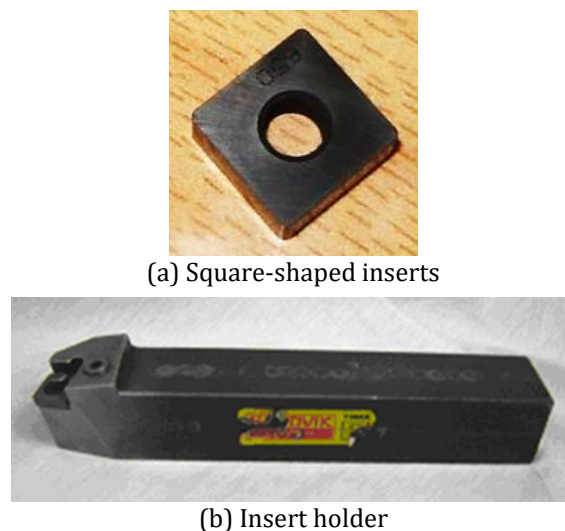


Fig. 2. Photographs of the insert and the insert-holder.

All relevant specifications of the cutting inserts are summarized in Table 2.

Table 2. The CC650 cutting inserts properties.

Cutting material	Firm	Firm designation
Mixed ceramics	Sandvik coramant	CC650
ISO Designation		Composition
SNGA12.04.08.T01020		70%AL2O3 + 30%TiC

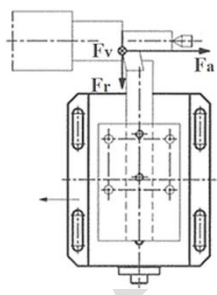
CC650 is a mixed ceramic grade based on alumina with added titanium carbide. It is primarily recommended for finishing operations on hardened steels, hardened cast irons, and refractory superalloys, offering a combination of high wear resistance and favorable thermal properties.

The geometry and specifications of the insert holder are provided in Table 3.

Table 3. Geometric characteristics of tool-holders.

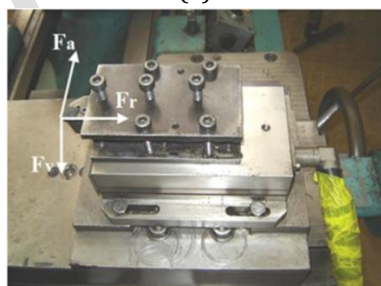
Insert-holder	χ ,°	α ,°	γ ,°	λ ,°	Section (mm)
PSBNR2525k12	75	6	-6	-6	25×25

Cutting force measurements were performed using a KISTLER dynamometer, a modern and highly reliable device for recording all three cutting force components. The measurement system consists of several elements, including the measurement platform (Fig. 3), a signal amplifier, a PC with dedicated software for data acquisition, and a printer for generating printed output of the recorded force curves (Fig. 4).



F_a : Axial force.
 F_r : Radial force.
 F_v : Tangential force.

(a)

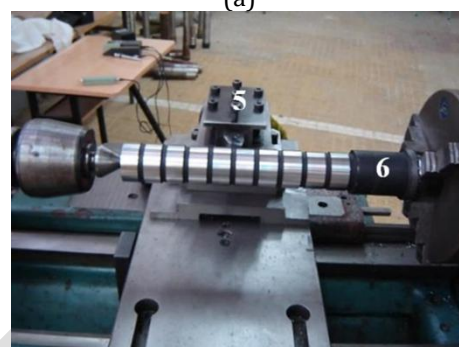


(b)

Fig. 3. (a) Basic principle, (b) Dynamometric tool holder type 9403.



(a)



(b)

Fig. 4. Cutting force measurement chain.

The measurement chain consists of the following components:

- 1) Microcomputer equipped with the Dynoware software.
- 2) Multichannel amplifier.
- 3) Connection cable linking the amplifier to the tool holder.
- 4) Printer for generating cutting force profiles.
- 5) Tool-holder platform.
- 6) Test specimen.

Surface roughness was evaluated using R_a for general process characterization, while R_z and R_t were monitored to detect local profile irregularities and ensure the functional integrity of the machined surfaces.

Surface roughness measurements (R_a , R_t , and R_z) were performed using a Mitutoyo SurfTest 301 2D roughness tester equipped with a profile printer. The device employs a diamond-tipped probe (5 μm tip radius) that moves linearly across the surface. The evaluation length (L_n) was set to 4 mm, based on a sampling length (λ_c) of 0.8 mm (0.8×5). This setup follows the standard configuration recommended by ISO 4288 (and ISO 21920-3) for surfaces with an expected arithmetic mean roughness (R_a) between 0.1 μm and 2 μm . The measurement range of the device is 0.05 to 40

μm for R_a and 0.3 to 160 μm for R_t and R_z . To minimize handling errors and improve accuracy, measurements were taken directly on the machine without dismantling the specimen (Fig. 5).

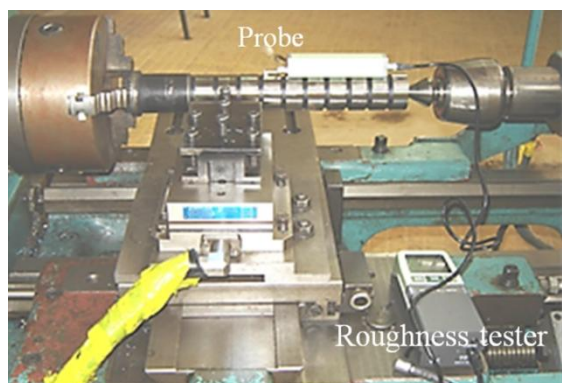


Fig. 5. Roughness tester in measurement position.

The hardness of the specimens was increased through heat treatment: quenching at 850 °C followed by tempering at 220 °C raised the material hardness to 60 HRC. The heat treatment properties of 100Cr6 steel are summarized in Table 4.

To comparatively investigate the evolution of cutting forces and surface roughness in conventional and hard turning, a series of dry turning tests was conducted on 100Cr6 steel in both the annealed and hardened states, using identical levels of cutting parameters. The specimens were mounted in a combined fixture throughout the tests.

Table 4. Heat treatment conditions of 100Cr6 steel.

Heat Treatment	Hardness	
	Before Heat Treatment	After Heat Treatment
Quenching at 850°C Tempering at 220°C	285HB~ 28,3 HRC	60HRC

The design of the experimental tests, based on the selected levels for each cutting parameter, is presented in Table 5. The selection of the experimental cutting conditions is based on industrial standards for finishing operations and tool manufacturer recommendations for AISI 52100 (100Cr6) steel. The cutting speed (V_c) range of 80 to 260 m/min was chosen to investigate the transition from mechanical dominance to thermal softening, particularly around the identified inversion point of 160 m/min. The feed rates (f) were restricted to

0.08–0.20 mm/rev to ensure surface finishes comparable to grinding standards. Finally, the depth of cut (ap) values (0.2 to 1 mm) were selected to analyze the influence of the tool nose radius on the radial force component (F_r), which is critical for the stability of hard turning processes.

Table 5. Experimental tests design.

Cutting conditions	Levels					Constant Levels
	80	120	160	200	260	
$V_c(\text{m/min})$	80	120	160	200	260	120
$f(\text{mm/rev})$	0.08	0.11	0.14	0.20	-	0.08
$ap(\text{mm})$	0.2	0.4	0.6	0.8	1	0.4

To ensure maximum reliability and reproducibility of the results, each experimental condition was repeated three to five times. The cutting force and surface roughness values reported in this work represent the arithmetic means of these independent trials. This rigorous approach confirms that the 20 mm machined length is sufficient to reach a stable steady-state, providing consistent data across all repetitions.

Furthermore, to isolate the influence of cutting parameters from tool degradation effects, flank wear was strictly monitored. A conservative replacement criterion was applied where the cutting edge was replaced as soon as the maximum flank wear (VB_{max}) approached 0.096 mm, ensuring it remained below the 0.1 mm threshold. A total of eight fresh ceramic cutting edges were utilized throughout the experimental campaign. This protocol ensured that all measurements for cutting forces, surface roughness, and chip morphology were captured under stable tool conditions, directly reflecting the influence of the cutting parameters.

Additionally, an analysis of chip morphology was performed to characterize both conventional and hard turning processes. The appearance of the chips provides valuable information on the evolution of plastic deformation in the machined material as a function of the cutting conditions.

Finally, mathematical models are required to describe the relationships between the cutting force components and surface roughness parameters with the cutting conditions. Based

on the curves of cutting forces and surface roughness as functions of cutting parameters (V_c , f , ap), the least squares method can be employed to derive mathematical models for the cutting force components in the following form:

$$F_{(Fa, Fr, Fv)} = C_3.Vc^x \quad (1)$$

$$F_{(Fa, Fr, Fv)} = C_2.f^y \quad (2)$$

$$F_{(Fa, Fr, Fv)} = C_1.ap^z \quad (3)$$

As well as mathematical models of surface roughness criteria:

$$R_{(Ra, Rt, Rz)} = C_3.Vc^x \quad (4)$$

$$R_{(Ra, Rt, Rz)} = C_2.f^y \quad (5)$$

$$R_{(Ra, Rt, Rz)} = C_1.ap^z \quad (6)$$

Where: C_1 , C_2 , C_3 are constants that take cutting conditions into account.

x , y , z : Exponents that indicate the degree of influence of each cutting condition (V_c , f , ap) on cutting force components and surface roughness criteria.

3. RESULTS AND DISCUSSION

The experimental results are presented and analyzed in this section to highlight the transition mechanisms between conventional and hard turning. The analysis begins with the evolution of cutting forces and surface topography, followed by a detailed examination of chip morphology to provide a physical basis for the observed trends. Finally, mathematical models are derived to quantify these relationships and facilitate process prediction.

A reliable evaluation of the influence of cutting parameters on cutting forces and surface roughness in both conventional and hard turning of 100Cr6 steel requires strict control of the material hardness. In this study, the measured hardness ranged from 31 to 35 HRC in the annealed state and 60 to 62 HRC in the hardened state.

As a reminder, the cutting force amplitudes recorded by the KISTLER dynamometer are processed using the Dynoware software, which converts the acquired signals into spectrometric curves displayed on the microcomputer (Fig. 6).

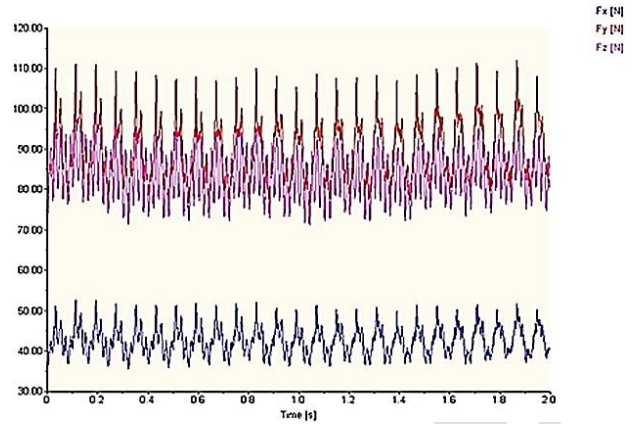


Fig. 6. Spectrometric curve of the cutting force components measured at a cutting speed of $V_c = 120$ m/min.

Initially, Figs. 7, 8, and 9 respectively illustrate the trends in the evolution of the axial force (Fa), radial force (Fr), and tangential force (Fv) as a function of the different levels of cutting parameters, including cutting speed, feed rate, and depth of cut, during conventional and hard turning.

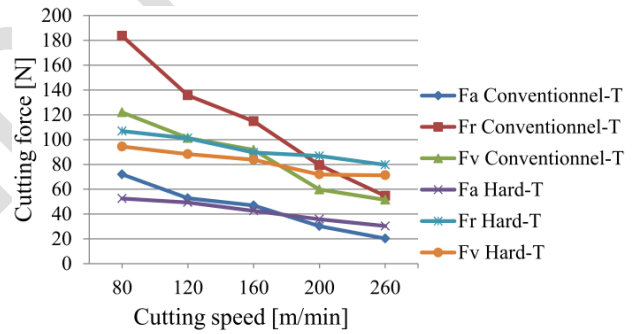


Fig. 7. Cutting force components as a function of cutting speed in conventional and hard turning ($f = 0.08$ mm/rev, $ap = 0.4$ mm).

Figure 8 shows that, at low cutting speeds, the cutting force components obtained in conventional turning are higher than those recorded in hard turning. At $V_c = 80$ m/min, the ratios between conventional and hard turning are 1.36, 1.71, and 1.29 for Fa , Fr , and Fv , respectively. However, beyond $V_c = 160$ m/min, the trend is reversed: the cutting forces measured during the machining of hardened 100Cr6 steel become higher than those obtained in the annealed condition. At $V_c = 260$ m/min, the differences reach 1.49 for Fa , 1.45 for Fr , and 1.38 for Fv .

These variations are closely linked to the material's thermo-mechanical behavior. At low cutting speeds, the high ductility of the annealed steel leads to more significant plastic deformation

and a larger tool-chip contact area, which induces higher friction and cutting forces. Moreover, the strain hardening effect is more dominant in the annealed state at these speeds. Conversely, at high cutting speeds, the hardened steel (60 HRC) maintains high mechanical strength and intense abrasivity despite thermal softening. This resistance to chip formation, combined with the localized shear instability (saw-tooth chip formation), leads to higher cutting force components compared to the annealed state where thermal softening is more effective.

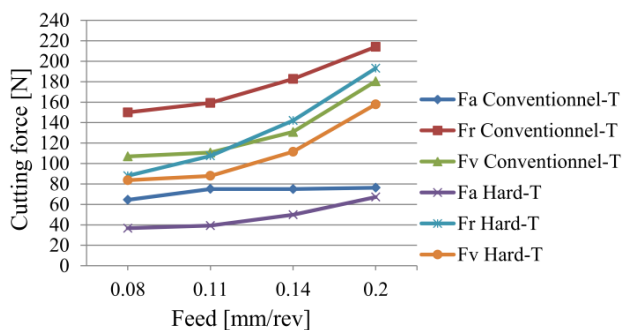


Fig. 8. Cutting force components as a function of feed rate in conventional and hard turning ($V_c = 120$ m/min, $a_p = 0.4$ mm).

The results show that the cutting forces in conventional turning are higher than those recorded in hard turning for all feed levels (Fig. 9). However, for the axial component, the trends of F_a in both machining conditions tend to converge as the feed increases. This behavior is attributed to a decrease in F_a before hardening and an increase in F_a after hardening of the 100Cr6 steel. Moreover, at a feed of $f = 0.08$ mm/rev, the axial cutting force in the annealed condition is 1.75 times higher than that obtained in the hardened condition. When the feed increases to $f = 0.20$ mm/rev, this difference is reduced to 1.13 times.

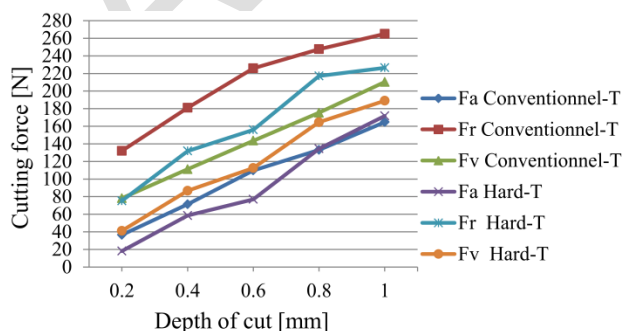
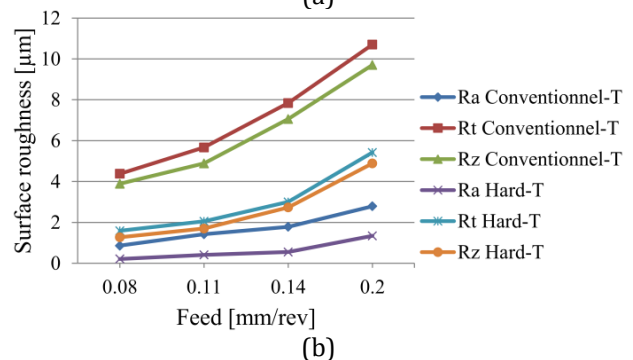
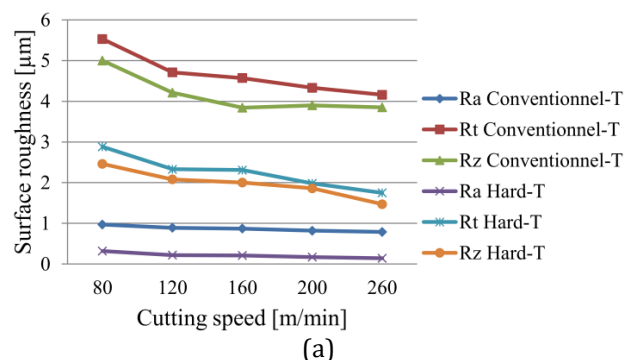


Fig. 9. Cutting force components as a function of depth of cut in conventional and hard turning ($V_c = 120$ m/min, $f = 0.08$ mm/rev).

In terms of depth of cut, the cutting force in conventional turning remains higher than that in hard turning (Fig. 10). However, the analysis shows that at $a_p = 0.2$ mm, the differences between conventional and hard turning are 2.00, 1.75, and 1.90 times for F_a , F_r , and F_v , respectively. At $a_p = 1$ mm, these ratios decrease to 0.959, 1.17, and 1.11, indicating that the cutting forces become nearly equivalent at larger depths of cut. Overall, while conventional turning generates higher forces at shallow depths of cut, the forces in both processes tend to converge as the depth of cut increases.

The thermo-mechanical equilibrium established by the cutting forces, particularly the dominance of the radial component (F_r), directly governs the stability of the tool-workpiece interface. This interaction is fundamentally responsible for the resulting surface topography, as the plastic deformation induced by these forces dictates the final roughness parameters (R_a , R_z , and R_t).

Secondly, the evolution of the surface roughness parameters R_a , R_t , and R_z as a function of the selected cutting parameters, including cutting speed, feed rate, and depth of cut, is shown in Figure 10 for both conventional and hard turning. These results allow us to assess the influence of the material condition (before and after hardening) on surface roughness at the different cutting parameter levels.



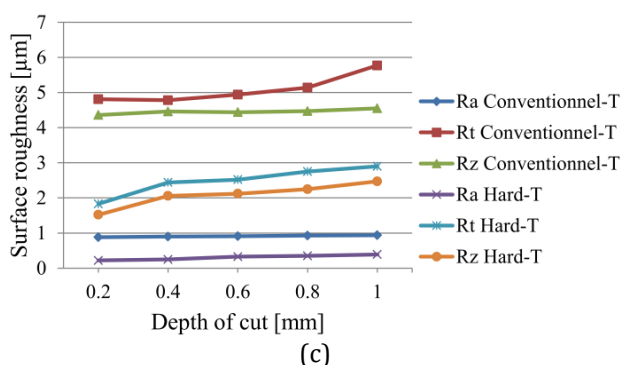


Fig. 10. Surface roughness parameters as a function of cutting conditions in conventional and hard turning: a) cutting speed, b) feed rate, and c) depth of cut.

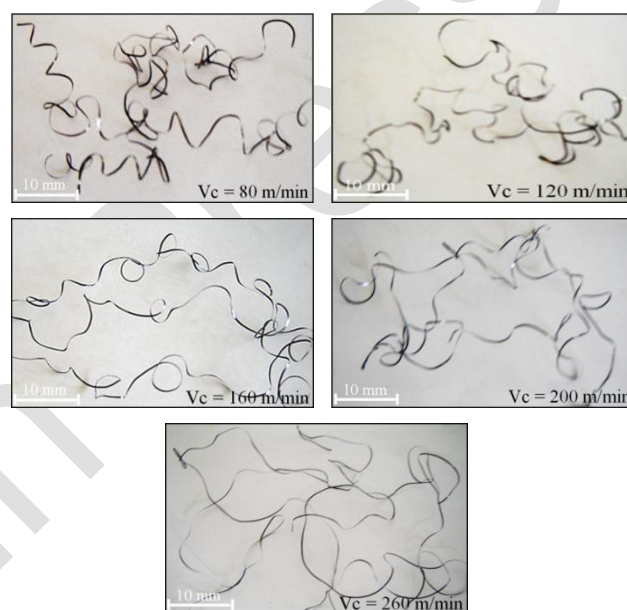
The improvement in surface quality is significant in hard turning compared to conventional turning. At a cutting speed of 260 m/min, surface roughness is reduced by factors of approximately 5.64, 2.37, and 2.61 for Ra , Rt , and Rz , respectively, at a feed rate of $f = 0.08$ mm/rev. For the same cutting speed, reductions are about 4, 2.75, and 3 times for the depth of cut $ap = 0.2$ mm.

The increased hardness of the machined material (60 HRC) implies a higher thermal stability of its microstructure compared to the annealed state. At high cutting speeds, although the rise in temperature promotes thermal softening (increasing ductility and elongation), the hardened 100Cr6 steel maintains a higher flow stress and mechanical resistance than the annealed steel [49,50]. This explains why the cutting forces for hard turning become higher than those recorded in the conventional turning condition beyond $V_c = 160$ m/min.

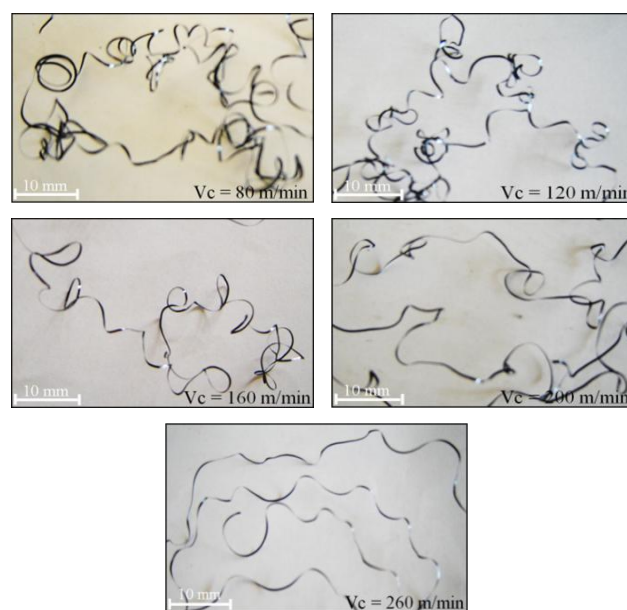
While the surface roughness provides an image of the final footprint left by the tool, the chip morphology serves as a dynamic signature of the cutting process itself. The transition from stable surface finishes to specific roughness profiles at high speeds is intrinsically linked to the chip formation mechanisms, shifting from continuous flow to localized shear instability.

Figures 11, 12, and 13 present the macroscopic chip morphology for both hard turning and conventional turning processes. While the chips remain continuous in both conditions, they differ significantly in their helix angles and curl radii. In conventional

turning, the high ductility of the annealed steel leads to disordered, ribbon-like chips. Conversely, the hardened steel (60 HRC) produces more regular helical chips, a result of the localized shear instability and reduced tool-chip contact length typical of hard machining. These observations are consistent with the force trends discussed previously and align with established chip formation models for AISI 52100 steel. To provide a physical reference, a 10 mm scale bar has been added to these macroscopic images.



(a) Annealed steel chip morphology



(b) Hardened steel chip morphology

Fig. 11. Morphology of chips at different cutting speeds ($f = 0.08$ mm/rev and $ap = 0.4$ mm).

For cutting speeds in the range of 80÷160 m/min, chips produced from the hardened material exhibit a more pronounced winding shape than those from annealed steel (Fig. 11a). This reduces friction at the cutting face, consequently lowering the cutting forces. This observation further supports the higher cutting forces recorded at low speeds when machining annealed steel. At higher speeds (200÷260 m/min), chips from the annealed material experience significant softening due to elevated temperatures, whereas chips from the hardened workpiece maintain their toughness and continue to exert higher pressures on the cutting face (Fig. 11b).

At a feed rate of $f = 0.08$ mm/rev during machining of hardened steel, the chips are continuous, thin, and exhibit a relatively large helix angle, which reduces the pressure on the cutting face and, consequently, the cutting forces. At a higher feed rate of $f = 0.20$ mm/rev, the chips become segmented, with a smaller radius of curvature, further reducing friction at the cutting edge and thereby lowering the cutting forces (Fig. 12).

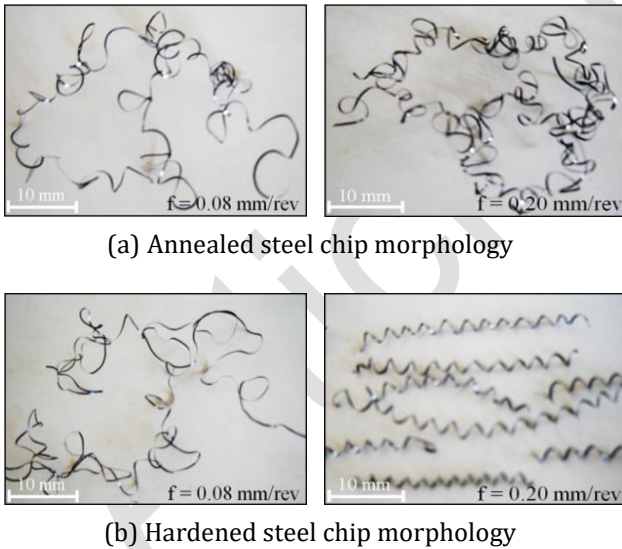


Fig. 12. Morphology of chips at different feeds ($V_c = 120$ m/min and $a_p = 0.4$ mm).

The chips shown in Fig. 13, produced during machining of 100Cr6 in the annealed state, are continuous and exhibit larger helix angles than those obtained from the hardened material. This observation helps explain the higher cutting force components recorded in conventional turning compared with hard turning, particularly at larger depths of cut.

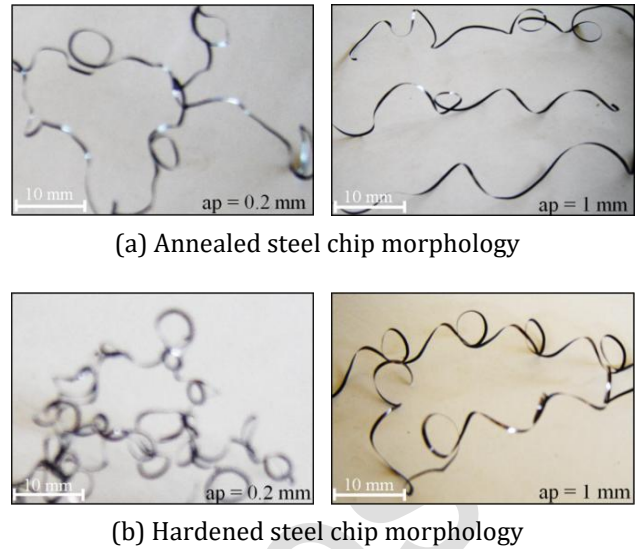


Fig. 13. Morphology of chips at different depths of cut ($V_c = 120$ m/min et $f = 0.08$ mm/rev).

Finally, to quantify the observed physical phenomena, mathematical models are required to describe the relationships between the cutting force components (Table 6), surface roughness parameters (Table 7), and the cutting conditions. By synthesizing the experimental trends of forces, roughness, and chip formation, the least squares method is employed to derive predictive models. These models bridge the gap between experimental observations and the final optimization goals discussed in the conclusion.

Table 6. Mathematical models and coefficient determination of cutting force components.

Cutting conditions		Mathematical models	R^2
Variable	Constant		
V_c (m/min)	f, a_p	$F_a = 56,723V_c^{-0,3313}$	0,8608
		$F_r = 109,62V_c^{-0,1797}$	0,9336
		$F_v = 97,241V_c^{-0,1855}$	0,8871
f (mm/tr)	V_c, a_p	$F_a = 33,833f^{0,4105}$	0,8130
		$F_r = 82,352f^{0,5443}$	0,9165
		$F_v = 76,274f^{0,4223}$	0,7672
a_p (mm)	f, V_c	$F_a = 19,229a_p^{1,3734}$	0,9851
		$F_r = 76,936a_p^{0,6977}$	0,9825
		$F_v = 42,057a_p^{0,9505}$	0,9924

The mathematical models based on a power-law formulation exhibit good to excellent correlation with the experimental data, as indicated by determination coefficients R^2 ranging from 0.76 to 0.99. The analysis shows that the depth of cut

ap is the most influential factor affecting the cutting forces, particularly the tangential force F_v , for which the models achieve the highest levels of fit. The cutting speed V_c predominantly affects the radial force F_r , while the feed rate f provides a significant yet more scattered contribution, leading to greater variability in F_v . Overall, these models reliably predict the evolution of cutting forces as a function of the machining parameters and represent a robust tool for optimizing the conventional and hard turning process of 100Cr6 steel.

Table 7. Mathematical models and coefficient of determination of surface roughness parameters.

Cutting conditions		Mathematical models	R ²
Variable	Constant		
V_c (m/min)	f, ap	$Ra = 0,3218V_c^{-0,4770}$	0,9566
		$Rz = 2,5278V_c^{-0,2726}$	0,8525
		$Rt = 2,9145V_c^{-0,2851}$	0,9289
f (mm/tr)	V_c, ap	$Ra = 0,1905f^{1,2191}$	0,9089
		$Rz = 1,1127f^{0,9232}$	0,8867
		$Rt = 1,4023f^{0,8237}$	0,8624
ap (mm)	f, V_c	$Ra = 0,2116ap^{0,3688}$	0,9509
		$Rz = 1,5748ap^{0,2794}$	0,9411
		$Rt = 1,8894ap^{0,2748}$	0,9554

The mathematical models obtained show an excellent predictive capability for the surface roughness parameters ($R^2 = 0.85-0.96$). The cutting speed (V_c) primarily influences R_a and R_t , with improved surface finish at higher speeds. The feed rate (f) remains the dominant factor in the formation of feed marks, which explains the slightly higher dispersion, although the models remain reliable. The depth of cut (ap) exhibits a consistent and significant effect, accompanied by the highest R^2 values, reflecting strong agreement between predictions and measurements. Overall, these models effectively predict surface roughness as a function of the cutting conditions and represent a robust tool for optimizing the machining of 100Cr6 steel in both conventional and hard turning.

The following conclusions synthesize the primary thermo-mechanical findings, the effectiveness of the predictive models, and their implications for transitioning from annealed to hard turning in industrial applications.

4. CONCLUSION

This study demonstrates that hard turning of 100Cr6 steel (60 HRC) offers significant advantages over conventional turning, especially for finishing operations. The specific findings are summarized as follows:

- **Cutting Force Hierarchy:** The radial force component is predominant ($F_r > F_v > F_a$) in both processes due to the small effective machining length relative to the tool nose radius.
- **Thermo-Mechanical Behavior:** A force inversion occurs at $V_c = 160$ m/min. Below this speed, conventional turning forces are higher due to material ductility by (36 %, 71 %, and 29 % for F_a , F_r , and F_v , respectively). Beyond this threshold, the superior thermal stability of hardened steel (60 HRC) maintains higher flow stress compared to the annealed state, with increases of 49 % for F_a , 45 % for F_r , and 38 % for F_v .
- **Surface Quality:** Hard turning consistently yields superior surface finishes. Optimal quality (R_a , R_z , and R_t) is achieved at high cutting speeds ($V_c = 260$ m/min) and low feed rates ($f = 0.08$ mm/rev).
- **Chip Morphology:** The transition from disordered ribbon-like chips in conventional turning to regular helical chips in hard turning reflects the shift from purely ductile deformation to localized shear instability.
- **Industrial Impact:** The results confirm that hard turning can effectively replace grinding, allowing for roughing and finishing on a single machine, thereby reducing production time and costs.

Future research will focus on investigating tool wear mechanisms and residual stress distribution to further evaluate surface integrity. Additionally, to deepen the understanding of the cutting process, microscopic investigations (SEM/EDX) of chip morphology will be conducted to analyze shear localization, saw-tooth formation, and the thermo-plastic instability mechanisms in hard turning. Finally, the implementation of Minimum Quantity Lubrication (MQL) will be explored to optimize the environmental sustainability of the process.

REFERENCES

- [1] R. Kumar, A. K. Sahoo, P. C. Mishra, R. K. Das, "Comparative investigation towards machinability improvement in hard turning using coated and uncoated carbide inserts: part I experimental investigation," *Advances in Manufacturing*, vol. 6, no. 1, pp. 52-70, Feb. 2018, doi: [10.1007/s40436-018-0215-z](https://doi.org/10.1007/s40436-018-0215-z)
- [2] D. I. Lalwani, N. K. MEHTA, and P. K. JAIN, "Experimental investigations of cutting parameters influence on cutting forces and surface roughness in finish hard turning of MDN250 steel," *Journal of materials processing technology*, vol. 206, no 1-3, pp. 167-179, Sep. 2008, doi: [10.1016/j.jmatprotec.2007.12.018](https://doi.org/10.1016/j.jmatprotec.2007.12.018)
- [3] M. O. Sahbi, S. Abdelhamid, M. A.Yallese, S. Belhadi, and A. Belamri, "Multi-Objective Optimization in Hard Turning of AISI 4140 Steel Using Taguchi-Based GRA and DEAR with Ceramic Tool," *Tribology in Industry*, vol. 47, no. 2, pp. 228-249, Mar. 2025, doi: [10.24874/ti.1842.12.24.03](https://doi.org/10.24874/ti.1842.12.24.03)
- [4] G. G. Lakić, B. Sredanović, D. Kramar, and J. Kopač, "Possibilities of application of high pressure jet assisted machining in hard turning with carbide tools," *Tribology in Industry*, vol. 39, no. 2, pp. 238-247. 2017, doi: [10.24874/ti.2017.39.02.11](https://doi.org/10.24874/ti.2017.39.02.11)
- [5] P. Umamaheswarrao, D. Rangaraju, K. N. S. Suman, and B. Ravisankar, "Machining force comparison for surface defect hard turning and conventional hard turning of AISI 52100 steel." *INCAS Bulletin*, vol. 13, no. 3, pp. 205-214. Feb. 2021, doi: [10.13111/2066-8201.2021.13.3.17](https://doi.org/10.13111/2066-8201.2021.13.3.17)
- [6] M. Q. Ibraheem, "Prediction of cutting force in turning process by using artificial neural network," *Al-Khwarizmi Engineering Journal*, vol. 16, no. 2, pp. 34-46. Apr 2020, doi: [10.22153/kej.2020.04.002](https://doi.org/10.22153/kej.2020.04.002)
- [7] H. Aouici, M. A. Yallese, K. Chaoui, T. Mabrouki, and J. F. Rigal, "Analysis of surface roughness and cutting force components in hard turning with CBN tool: Prediction model and cutting conditions optimization," *Measurement*, vol. 45, no. 3, pp. 344-353. Dec 2011, doi: [10.1016/j.measurement.2011.11.011](https://doi.org/10.1016/j.measurement.2011.11.011)
- [8] G. Bartarya, and S. K. Choudhury, "Effect of cutting parameters on cutting force and surface roughness during finish hard turning AISI52100 grade steel," *Procedia CirP*, vol. 1, pp. 651-656 2012, doi: [10.1016/j.procir.2012.04.116](https://doi.org/10.1016/j.procir.2012.04.116)
- [9] M. Boy, N. Yaşar, and İ. Çiftçi, "Experimental investigation and modelling of surface roughness and resultant cutting force in hard turning of AISI H13 steel," In : *IOP Conference Series: Materials Science and Engineering. IOP Publishing*, p. 012039, 2016, doi: [10.1088/1757-899X/161/1/012039](https://doi.org/10.1088/1757-899X/161/1/012039)
- [10] M. W. Azizi, S. Belhadi, M. A. Yallese, T. Mabrouki, and J. F. Rigal, "Surface roughness and cutting forces modeling for optimization of machining condition in finish hard turning of AISI 52100 steel," *Journal of mechanical science and technology*, vol. 26, no. 12, pp. 4105-4114, Jul. 2012, doi: [10.1007/s12206-012-0885-6](https://doi.org/10.1007/s12206-012-0885-6)
- [11] N. M. Tuan, T. T. Long, and T.B. Ngoc, "Study of Effects of MoS2 Nanofluid MQL Parameters on Cutting Forces and Surface Roughness in Hard Turning Using CBN Insert," *Fluids*, vol. 8, no. 7, pp. 188. Jun 2023, doi: [10.3390/fluids8070188](https://doi.org/10.3390/fluids8070188)
- [12] H. A. Çetindağ, A. Çiçek, N. Uçak, and K. Aslantas, "Performance of conventional and wiper CBN inserts under various cooling conditions in hard turning of AISI 52100 steel," *Materials Testing*, vol. 66, no. 2, pp. 288-298, 2024, doi: [10.1515/mt-2023-0263](https://doi.org/10.1515/mt-2023-0263)
- [13] B. Hamadi, M. A. Yallese, L. Boulanouar, M. Nouioua, and A. Hammoudi, "RSM-based MOALO optimization and cutting inserts evaluation in dry turning of AISI 4140 steel," *Struct Eng Mech*, vol. 84, no. 1, pp. 17-33. Oct. 2022, doi: [10.12989/sem.2022.84.1.017](https://doi.org/10.12989/sem.2022.84.1.017)
- [14] S. K. Thangarasu, S. SHANKAR, and K. Devendran, "Tool wear prediction in hard turning of EN8 steel using cutting force and surface roughness with artificial neural network," *Proceedings of the Institution of Mechanical Engineers, Part C: Journal of Mechanical Engineering Science*, vol. 234, no. 1, pp. 329-342, 2020, doi: [10.1177/0954406219873932](https://doi.org/10.1177/0954406219873932)
- [15] K. Osička, J. Zouhar, P. Sliwková, and J. Chladil, "Cutting Force When Machining Hardened Steel and the Surface Roughness Achieved," *Applied Sciences*, vol. 12, no. 22, p. 11526, Nov 2022, doi: [10.3390/app122211526](https://doi.org/10.3390/app122211526)
- [16] M. Özdemir, M. Kaya, and H. Akyildiz, "Analysis of surface roughness and cutting forces in hard turning of 42CrMo4 steel using Taguchi and RSM method," *Mechanika*, vol. 26, no. 3, pp. 231-241, Jun. 2020, doi: [10.5755/j01.mech.26.3.23600](https://doi.org/10.5755/j01.mech.26.3.23600)
- [17] R. Kumar, A. K. Sahoo, P. C. Mishra, R. K. Das, and M. Ukamanal, "Experimental investigation on hard turning using mixed ceramic insert under accelerated cooling environment," *International Journal of Industrial Engineering Computations*, vol. 9, no. 4, pp. 509-522, Nov. 2018, doi: [10.5267/j.ijiec.2017.11.002](https://doi.org/10.5267/j.ijiec.2017.11.002)
- [18] S. Mane, and H. Vasudevan, "Experimental Investigation, Modeling, and Optimization of Cutting Forces in Dry Hard Turning," In : *Proceedings of International Conference on*

- Intelligent Manufacturing and Automation: ICIMA 2022*. Singapore: Springer Nature Singapore, pp. 481-489, Mar. 2023, doi: [10.1007/978-981-19-7971-2_46](https://doi.org/10.1007/978-981-19-7971-2_46)
- [19] S. R. Das, A. Kumar, and D. Dhupal, "Experimental investigation on cutting force and surface roughness in machining of hardened AISI 52100 steel using cBN tool," *International Journal of Machining and Machinability of Materials*, vol. 18, no. 5-6, pp. 501-521, Sep. 2016, doi: [10.1504/IJMMM.2016.078997](https://doi.org/10.1504/IJMMM.2016.078997)
- [20] V. R. Balwan, B. Dabade, and L. Wankhade, "Influence of hard turning parameters on cutting forces of EN 353 steel," *Materials Today: Proceedings*, vol. 63, pp. 149-156, 2022, doi: [10.1016/j.matpr.2022.02.425](https://doi.org/10.1016/j.matpr.2022.02.425)
- [21] S. Kumar, P. Tamilselvan, M. Feroskhan, A.S.A. Doss, M. Sasikumar, M. Elango, and S. Sivarajan, "Hard turning of AISI D2 steel with cubic boron nitride cutting inserts," *Materials Today: Proceedings*, vol. 72, pp. 2002-2006, 2023, doi: [10.1016/j.matpr.2022.07.338](https://doi.org/10.1016/j.matpr.2022.07.338)
- [22] M. T. Ngol, "Influence of technology parameters on the total cutting force in the hard turning process with NF MQL and NF MQCL method using nanofluids," *Tribology in Industry*, Vol. 45, no. 2, pp. 272-284, May. 2023, doi: [10.24874/ti.1453.02.23.05](https://doi.org/10.24874/ti.1453.02.23.05)
- [23] R. Kumar, A. K. Sahoo, P. C. Mishra, and R. K. Das, "Investigation on tool wear and surface characteristics in hard turning under air-water jet spray impingement cooling environment," *Tribology in Industry*, vol. 41, no. 2, pp. 172-187, 2019, doi: [10.24874/ti.2019.41.02.04](https://doi.org/10.24874/ti.2019.41.02.04)
- [24] X. Wang, M. Yang, T. Gao, L. Dong, Y. S. Dambatta, X. Liu, Y. Yang, Q. An, Y. Zhang, C. Li, "Lubricant transport mechanism and dynamics model for nepenthes-shaped biomimetic microtexture," *Chinese Journal of Mechanical Engineering*, vol. 38, no. 1, p. 36, 2025, doi: [10.1186/s10033-025-01197-8](https://doi.org/10.1186/s10033-025-01197-8)
- [25] L. Sun, Y. Zhang, S. Xu, X. Cui, Q. An, Y. Chen, D. Jia, C. Zhang, C. Li, "Modelling and heat transfer mechanism of coated tool temperature field in sustainable turning based on the finite difference method," *Applied Thermal Engineering*, vol. 267, p. 125803, 2025, doi: [10.1016/j.applthermaleng.2025.125803](https://doi.org/10.1016/j.applthermaleng.2025.125803)
- [26] Y. Shi, B. Zhao, W. Ding, "Solid additives to increase the service life of ceramic cutting tool: methodology and mechanism," *Intelligent and Sustainable Manufacturing*, vol. 1, no. 2, p. 10009, 2024, doi: [10.35534/ism.2024.10009](https://doi.org/10.35534/ism.2024.10009)
- [27] X. Wang, C. Li, Y. Zhang, H. M. Ali, S. Sharma, R. Li, M. Yang, Z. Said, X. Liu, "Tribology of enhanced turning using biolubricants: A comparative assessment," *Tribology International*, vol. 174, p. 107766, 2022, doi: [10.1016/j.triboint.2022.107766](https://doi.org/10.1016/j.triboint.2022.107766)
- [28] P. Gong, Y. Zhang, X. Cui, S. Xu, M. Yang, D. Jia, C. Li, "Lubricant transportation mechanism and wear resistance of different arrangement textured turning tools," *Tribology International*, vol. 196, p. 109704, 2024, doi: [10.1016/j.triboint.2024.109704](https://doi.org/10.1016/j.triboint.2024.109704)
- [29] T. B. Ngoc, T. M. Duc, N. M. Tuan, T. T. Long, "Influence of Al₂O₃/MoS₂ hybrid nanofluid MQL on surface roughness, cutting force, tool wear and tool life in hard turning," *Forces in Mechanics*, vol. 16, p. 100285, Aug. 2024, doi: [10.1016/j.finmec.2024.100285](https://doi.org/10.1016/j.finmec.2024.100285)
- [30] C. H. Mimoun, K. Haddouche, S. Makhfi. "Predicting the Resultant Cutting Force in Hard Turning Using Machine Learning Techniques," *Engineering, Technology & Applied Science Research*, vol. 15, no. 5, pp. 26505-26510, Oct. 2025, doi: [10.48084/etasr.11759](https://doi.org/10.48084/etasr.11759)
- [31] V. Sharma, P. Kumar, J. P. Misra, "Cutting force predictive modelling of hard turning operation using fuzzy logic," *Materials Today: Proceedings*, vol. 26, pp. 740-744, 2020, doi: [10.1016/j.matpr.2020.01.018](https://doi.org/10.1016/j.matpr.2020.01.018)
- [32] D. Abdelhakim, F. Harrou, Y. Sun, S. Makhfi, M. Habak, "Explainable machine learning for enhancing predictive accuracy of cutting forces in hard turning processes," *The International Journal of Advanced Manufacturing Technology*, vol. 135, no. 1, pp. 939-961, Oct. 2024, doi: [10.1007/s00170-024-14470-2](https://doi.org/10.1007/s00170-024-14470-2)
- [33] R. Kumar, M. Rafiqhi, M. Özdemir, A. Şahinoğlu, A. Kulshreshta, J. Singh, S. Singh, C. Prakash, A. Bhowmik, "Modeling and optimization of hard turning: predictive analysis of surface roughness and cutting forces in AISI 52100 steel using machine learning," *International Journal on Interactive Design and Manufacturing (IJIDeM)*, vol. 19, no. 8, pp. 5749-5778, 2025, doi: [10.1007/s12008-024-02166-6](https://doi.org/10.1007/s12008-024-02166-6)
- [34] S. Chinchani, O. Kulkarni, P. Dhond, M. Kumawat, S. Chaudhari, "Investigating Cutting Forces During Hard Turning of EN 24 Steel: A Comparative Evaluation of MQL and Dry Cutting," *In International Conference on Futuristic Advancements in Materials, Manufacturing and Thermal Sciences*, pp. 73-83. Singapore: Springer Nature Singapore, Jan. 2024, doi: [10.1007/978-981-97-4324-7_6](https://doi.org/10.1007/978-981-97-4324-7_6)
- [35] A. Tzotzis, N. Tapoglou, R. K. Verma, P. Kyratsis, "3D-FEM approach of AISI-52100 hard turning: modelling of cutting forces and cutting condition optimization," *Machines*, vol. 10, no. 2, p. 74, Jan. 2022, doi: [10.3390/machines10020074](https://doi.org/10.3390/machines10020074)

- [36] A. Zawada-Tomkiewicz, E. Zeuschner, "Surface roughness in hard turning of EN 100Cr6 with coated PCBN cutting tools at micro cutting depths," *The International Journal of Advanced Manufacturing Technology*, vol. 139, no. 11, pp. 5545-5561, Aug. 2025, doi: [10.1007/s00170-025-16186-3](https://doi.org/10.1007/s00170-025-16186-3)
- [37] S. Mane, R. B. Patil, A. Roy, P. Shah, R. Sekhar, "Analysis of the Surface Quality Characteristics in Hard Turning Under a Minimal Cutting Fluid Environment," *Applied Mechanics*, vol. 6, no. 1, p. 5, 2025, doi: [10.3390/applmech6010005](https://doi.org/10.3390/applmech6010005)
- [38] J. Jacob, M. Meurer, T. Bergs, "Surface Roughness Prediction in Hard Turning (Finishing) of 16MnCr5 Using a Model Ensemble Approach," *Procedia CIRP*, vol. 126, pp. 504-507, 2024, doi: [10.1016/j.procir.2024.08.409](https://doi.org/10.1016/j.procir.2024.08.409)
- [39] T. P. Gundarneeeya, V. D. Golakiya, S. D. Ambaliya, S. H. Patel, "Experimental investigation of process parameters on surface roughness and dimensional accuracy in hard turning of EN24 steel," *Materials Today: Proceedings*, vol. 57, pp. 674-680, 2022, doi: [10.1016/j.matpr.2022.02.104](https://doi.org/10.1016/j.matpr.2022.02.104)
- [40] A. Muqet, A. Israr, M. H. Zafar, M. Mansoor, N. Akhtar, "A novel optimization algorithm based PID controller design for real-time optimization of cutting depth and surface roughness in finish hard turning processes," *Results in Engineering*, vol. 18, p. 101142, Jun. 2023, doi: [10.1016/j.rineng.2023.101142](https://doi.org/10.1016/j.rineng.2023.101142)
- [41] M. S. Karthik, V. R. Raju, K. N. Reddy, N. Balashanmugam, M. R. Sankar, "Cutting parameters optimization for surface roughness during dry hard turning of EN 31 bearing steel using CBN insert," *Materials Today: Proceedings*, vol. 26, pp. 1119-1125, 2020, doi: [10.1016/j.matpr.2020.02.224](https://doi.org/10.1016/j.matpr.2020.02.224)
- [42] N. Ambhore, D. Kamble, S. Chinchankar, "Evaluation of cutting tool vibration and surface roughness in hard turning of AISI 52100 steel: an experimental and ANN approach," *Journal of Vibration Engineering & Technologies*, vol. 8, no. 3, pp. 455-462, 2020, doi: [10.1007/s42417-019-00136-x](https://doi.org/10.1007/s42417-019-00136-x)
- [43] M. Neslušán, J. Uríček, A. Mičietová, P. Minárik, M. Píška, M. Čilliková, "Decomposition of cutting forces with respect to chip segmentation and white layer thickness when hard turning 100Cr6," *Journal of Manufacturing Processes*, vol. 50, pp. 475-484, Feb. 2020, doi: [10.1016/j.jmapro.2020.01.004](https://doi.org/10.1016/j.jmapro.2020.01.004)
- [44] R. R. Lenka, A. Jena, L. R. Bhandarkar, S. K. Sarangi, "Dynamic chip morphology study of AISI 52100 by advanced coated cutting tools." *Sādhanā*, vol. 51, no. 1, p. 9, Jan. 2026, doi: [10.1007/s12046-025-03023-2](https://doi.org/10.1007/s12046-025-03023-2)
- [45] V. Y. Lebedev, V. E. Babich, Y. A. Ziziko, N. V. Lebedev, "Features of Chip Formation and Wear of Blades Made of Superhard Materials Based on CBN during Turning Hardened Steels," *Surface Engineering and Applied Electrochemistry*, vol. 61, no. 4, pp. 492-499, Sep. 2025, doi: [10.3103/S1068375525700498](https://doi.org/10.3103/S1068375525700498)
- [46] S. Fujian, Y. Junhao, L. Zhiqiang, L. Yanjun, C. Jinlong, X. Gang, L. Xuezhi, X. Yubin, H. Hao, Y. Jianping, "Enhancement of machinability and surface tribological property of hardened bearing steel by electric pulse-assisted hard turning," *Tribology International*, vol. 199, p. 110022, Nov. 2024, doi: [10.1016/j.triboint.2024.110022](https://doi.org/10.1016/j.triboint.2024.110022)
- [47] S. Roy, S. Swain, A. Das, S. R. Das, "Performance of AlTiN-and AlTiSiN-Coated Carbide Tools in Dry Turning of Hardened AISI 4140 Steel: A Comparative Investigation," *Journal of Materials Engineering and Performance*, pp. 2971-2992, 2026, doi: [10.1007/s11665-025-11710-8](https://doi.org/10.1007/s11665-025-11710-8)
- [48] E. Abdelnasser, S. El-Sanabary, A. Nassef, A. Barakat, A. Elkaseer, "Influence of technological parameters on chip formation and chip control in precision hard turning of Ti-6Al-4V," *Micromachines*, vol. 14, no. 10, p. 1973, 2023, doi: [10.3390/mi14101973](https://doi.org/10.3390/mi14101973)
- [49] K. Bouacha, M. A. Yallese, T. Mabrouki, J. F. Rigal, "Statistical analysis of surface roughness and cutting forces using response surface methodology in hard turning of AISI 52100 bearing steel with CBN tool," *International Journal of Refractory Metals and Hard Materials*, vol. 28, no. 3, pp. 349-361, May. 2010, doi: [10.1016/j.ijrmhm.2009.11.011](https://doi.org/10.1016/j.ijrmhm.2009.11.011)
- [50] G. Poulachon, A. Albert, M. Schluraff, I. S. Jawahir, "An experimental investigation of work material microstructure effects on white layer formation in PCBN hard turning," *International Journal of Machine Tools and Manufacture*, vol. 45, no. 2, pp. 211-218, 2005, doi: [10.1016/j.ijmachtools.2004.07.009](https://doi.org/10.1016/j.ijmachtools.2004.07.009)